applied optics

Sub-megahertz frequency stabilization of a diode laser by digital laser current modulation

JIAMING LI,[1,2] JI LIU,[1] LEONARDO DEMELO,[1] LE LUO,[1,*] TIANSHU LAI,[2,3] AND ZIXIN WANG[2,4]

[1]Department of Physics, Indiana University Purdue University Indianapolis, Indianapolis, Indiana 46202, USA
[2]School of Physics and Engineering, Sun Yat-sen University, Guangzhou 510275, China
[3]e-mail: stslts@mail.sysu.edu.cn
[4]e-mail: wangzix@mail.sysu.edu.cn
*Corresponding author: leluo@iupui.edu

Received 28 January 2015; accepted 22 March 2015; posted 26 March 2015 (Doc. ID 233220)

Digital laser current modulation (DLCM) is a convenient laser stabilization scheme whose major advantages are simplicity and inexpensiveness of implementation. However, there is a tradeoff between the SNR of the error signal and the laser linewidth due to the direct laser frequency modulation. In this paper, we demonstrated that DLCM can reduce the FWHM linewidth of a tunable diode laser down to 500 kHz using the modulation transfer spectrum of D_2 line of a ^{6}Li atomic vapor. For this purpose, a theoretical model is provided to analyze the DLCM-based modulation transfer spectrum. From the analysis, we experimentally explored the modulation effect on the DLCM spectrum to minimize the laser linewidth. Our result shows the optimized DLCM can stabilize a diode laser into the sub-megahertz regime without requiring acousto-optic and electro-optic modulators.

OCIS codes: (140.3425) Laser stabilization; (020.3690) Line shapes and shifts; (300.6290) Spectroscopy, four-wave mixing.

http://dx.doi.org/10.1364/AO.99.099999

1. INTRODUCTION

Active frequency stabilization of a tunable single-frequency diode laser plays an important role in many atomic physics experiments, such as magneto-optical trap and absorption imaging [1,2]. A broad range of experimental setups employ an atomic vapor cell for locking the laser frequency to a Doppler-free spectrum, where the modulated pump and/or probe beams are applied to generate the error signals for locking. The modulation techniques are quite varied, including laser current modulation spectroscopy (LCMS) [3], electro-optic frequency modulation spectroscopy (EOFMS) [4–6], acousto-optic modulation transfer spectroscopy (AOMTS) [7–9], and their recent variants such as acousto-optic frequency modulation spectroscopy (AOFMS) [10], piezo frequency modulation spectroscopy (PFMS) [11], and so on.

EOFMS is one of the most widely used methods to stabilize the laser frequency, requiring expensive EOMs and radio-frequency (RF) devices to generate the sideband frequencies of the probe beam. AOMTS modulates the frequency of the pump beam instead of the probe beam to reduce the noise in the detected signal. It usually stabilizes the laser linewidth at the megahertz (MHz) regime due to the stability of the voltage-controlled oscillator (VCO) of the acousto-optic modulation (AOM) driver [10]. To improve the locking stability of AOMTS down to the sub-MHz level, a customized wideband VCO is implemented [9]. For a tunable diode laser, both EOFMS and AOMTS can be replaced by diode current modulation for generating sideband frequencies [12]. Comparing to AOMTS and EOFMS, digital laser current modulation (DLCM) is a simpler method, but it is challenging to obtain sub-MHz laser frequency stability because of two difficulties: first the laser frequency noise will be increased by directly modulating the laser current, and second the laser linewidth will be broadened by sideband frequencies. To address these problems, we simulated the DLCM-based modulation transfer spectrum to estimate the modulation effect, which helps us to narrow the laser linewidth down to 500 kHz by optimizing the modulation frequency, the modulation amplitude, and the servo bandwidth.

The paper is organized as follows. In Section 2, we describe the experimental setup that stabilizes a Toptica Photonic TA laser with the DLCM-based Doppler-free spectroscopy of a hot lithium vapor cell. In Section 3, we present a theoretical model to simulate the DLCM spectrum. In Section 4, we prrsent the measured DLCM spectrum and laser linewidth to determine the optimized modulation parameters. Finally, we summarize the results and discuss the relevant applications.

2. EXPERIMENTAL SETUP

DLCM is applied to an external cavity diode laser with a tapered amplifier (ECDL1, Toptica Photonic TA Pro) as shown in Fig. 1. A 1.6 mW beam from the ECDL1 is divided by a polarizing beamsplitter: one beam for the Doppler-free spectroscopy of a ^{6}Li vapor cell and the other for generating the beating signals with an offset-locking laser (ECDL2, Toptica Photonic DL 100 Pro) to measure the laser linewidth. For the DLCM spectrum from the vapor, the retro-reflected pump beam is used as the probe beam and detected by a homemade photodetector (PD), which has 10^5 gain and 6 MHz bandwidth with electronic noise of 300 $\mathrm{nV}\cdot\mathrm{Hz}^{-1/2}$ at 100 kHz. The lithium vapor cell is heated to 340 ± 1°C, and the resonant absorption ratio of the ^{6}Li D_2 line is about 0.5. In order to reduce the magnetic field generated by the heating coil, a single-core heating element tape is uniformly wrapped and divided into two layers with opposite current directions. The measured magnetic field inside the cell is 100 ± 10 mG. The fluctuation of the magnetic field corresponds to about 30 kHz Zeeman shift of the ground state 2 $^2S_{1/2}$, $F = 3/2$ of ^{6}Li, which cause negligible effects for the locking at hundreds of kilohertz (kHz) level. To compare the laser locking performance between DLCM and AOFMS, the laser beam can also be forwarded to a double-passed AOM for AOFMS. The digital laser current modulation is realized by modulating the diode current through a DigiLock 110 module (Toptica Photonic). The clock rate of this module is 100 MHz, providing the maximum modulation frequency of 25 MHz and the maximum servo loop bandwidth of 10 MHz. For DLCM, the modulation sideband frequencies exist in both the pump and probe beams, generating the DLCM spectrum by four-wave mixing in the atomic vapor [13,14]. The spectrum is then electronically demodulated by the DigiLock module for locking error signal. A digital low-pass filter (LPF) with the bandwidth of the half of the modulation frequency is put before the proportional–integral–derivative (PID) controllers to remove the high-frequency components. Such high-frequency components cannot be suppressed by the servo loop according to the Nyquist–Shannon sampling theorem [15]. After the LPF, the error signal is sent to two PID modules separately, where PID1 controls the piezoelectric transducer (PZT) of the ECDL1 with the cut-off frequency of 1 kHz, and PID2 adjusts the current of the diode.

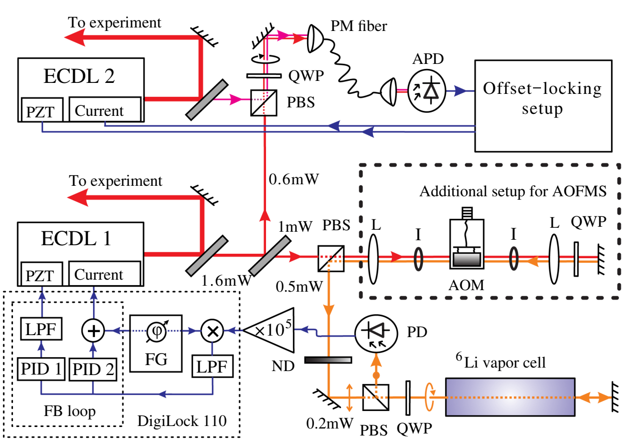

Fig. 1. Experimental setup of the DLCM laser locking. APD, avalanche photodetector; FB loop, feedback loop; FG, function generator; I, iris; L, lens; ND, neutral density filter; PM fiber, polarization-maintaining single-mode fiber; PBS, polarizing beamsplitter; PD, photodetector; PZT, piezoelectric transducer; QWP, quarter waveplate.

3. SPECTRUM MODELING

The sideband frequencies of the DLCM are generated by modulating the diode current with frequency ω_m, giving the electric field of the laser output as

$$E(t) = \frac{E_0}{2} \exp[i(\omega_0 t + \beta \sin(\omega_m t))] + \text{c.c.}$$
$$= \frac{E_0}{2} \sum_{n=-\infty}^{+\infty} J_n(\beta) e^{i(\omega_0 + n\omega_m)t} + \text{c.c.}, \tag{1}$$

where $\beta = \Delta\omega/\omega_m$ is the modulation index, $\Delta\omega$ is the modulation amplitude, and $J_n(\beta)$ is the nth-order Bessel function. DLCM modulates both the pump and probe beams for generating modulation transfer spectrum though a four-wave mixing process in an atomic vapor cell. This is similar to AOMTS [7,14], where the amplitude modulation of the probe beam is generated from the frequency modulation of the pump beam through a four-wave mixing process in the atomic vapor [8,9]. For efficient four-wave mixing, ω_m must be within the frequency range of the Doppler-free feature.

When both the pump and probe beams are modulated, the four-wave mixing process involves multiple frequency sidebands. The amplitude-modulated probe signal recorded by the photodetector is described by [14]

$$S = C \sum_{m,m',n,n'=-\infty}^{+\infty} J_m(\beta) J_{m'}(\beta) J_n(\beta) J_{n'}(\beta) \times \mathrm{Re}\left\{ \frac{\exp[i(m - m' + n - n')\omega_m t]}{\Gamma + i(n - n')\omega_m} \times \frac{1}{2\Gamma - 2i\Delta - i(m' + 2n' - n)\omega_m} \right\}, \tag{2}$$

where Δ is the laser frequency detuning from the resonant frequency, Γ is the spectrum linewidth, $J_n(\beta)$ and $J_{n'}(\beta)$ are the amplitude coefficients of two sidebands of the pump beam, $J_{m'}(\beta)$ and $J_m(\beta)$ are the coefficients of the probe beam, and J_n, $J_{n'}$, and $J_{m'}$ represent the incoming waves of the four-wave mixing process. $J_m(\beta)$ represents the beating wave with the outcoming wave. When the modulation index is much larger than the unity, Eq. (2) includes many terms. For example, a modulation index of 10 makes 29 Bessel terms with more than 1% contribution to the DLCM signal.

In practice, only the first-order of the modulation frequency in the DLCM signal is electronically demodulated for locking, so we restrict $(m - m') - (n - n') = \pm 1$. The first-order signal of Eq. (2) can be simplified as a combination of Lorentzian and dissipative profile [7,16] as follows

$$S = C \sum_{m',n,n'=-\infty}^{+\infty} \frac{J_{m'}(\beta) J_n(\beta) J_{n'}(\beta)}{\Gamma^2 + ((n - n')\omega_m)^2} \times \left[(J_{m_+}(\beta) + J_{m_-}(\beta)) L_{\frac{m'}{2}+n'-\frac{n}{2}}(\Delta) \cos(\omega_m t + \phi) + (J_{m_+}(\beta) - J_{m_-}(\beta)) D_{\frac{m'}{2}+n'-\frac{n}{2}}(\Delta) \sin(\omega_m t + \phi) \right], \tag{3}$$

where

$$L_n(\Delta) = \frac{\Gamma^2}{\Gamma^2 + (\Delta - n\omega_m)^2}, \tag{4}$$

$$D_n(\Delta) = \frac{\Gamma(\Delta - n\omega_m)}{\Gamma^2 + (\Delta - n\omega_m)^2},$$

where $m_\pm = m' + n' - n \pm 1$ for the $\pm\omega_m$ sidebands of the demodulated signal, and ϕ is the phase difference between the DLCM signal and the local oscillation.

4. MEASUREMENT AND RESULT

To optimize the DLCM locking, we first optimize the modulation parameters, including the modulation index and the modulation frequency, to improve the SNR of the DLCM spectrum. Then we minimize the laser linewidth by tuning these modulation parameters. Finally we studied long-term stability of the locking.

A. DLCM Spectrum Measurement

The DLCM spectrum is obtained on the $2\,^2S_{1/2}, F = 3/2$ to $2\,^2P_{3/2}$ transition of ^{6}Li. The pump beam is 200 μW with 0.8 mm beam waist. The retro-reflected beam is used as the probe beam, which has 100 μW due to the vapor absorption. In Fig. 2, a typical spectrum with $\Delta\omega = 0.8$ MHz and $\omega_m = 100$ kHz is represented by the thin black curve. The laser current modulation amplitude $\Delta\omega$ is calibrated by additional AOFMS with known frequency modulation amplitudes. The spectrum curve is taken at 4 kHz sampling rate by scanning the PZT of ECDL1 in 50 ms to reduce the PZT thermal drift. The thick black curve is the fitting using Eq. (3), where the fitted linewidth $\Gamma = 2\pi \cdot 10.9$ MHz, in agreement with the combination of the 5.9 MHz natural linewidth of ^{6}Li D_2 transition and the 4.4 MHz separation between three hyperfine states of the excited levels.

We compared the DLCM spectrum with the AOFMS spectrum by implementing an independent acousto-optic (AO) frequency modulation. The thin red curve in Fig. 2 shows the AOFMS spectrum with the same modulation parameters as the DLCM one. We found that the SNR of the DLCM spectrum is about 3 times higher than the AOFMS one. It is also shown that the DLCM spectrum has much lower residual amplitude modulation (RAM) effect than the AOFMS one, indicated by the frequency asymmetry of the spectrum. These findings imply that DLCM, even though the laser itself is frequency-modulated, may result in a better locking performance than AOFMS in certain modulation conditions.

B. Laser Linewidth Measurement

To measure the laser linewidth, the DLCM-stabilized laser beats with the other diode laser ECDL2 locked by the offset-locking [18], as shown in Fig. 3(a). Two laser beams are coupled into a PM fiber to improve the SNR of the beating signal. A high-speed APD (Newport 877) with two low-noise RF amplifiers (Miniciruit ZX60-3018G+) is applied to probe the beating signal, where 1 of the beating signal is used for the linewidth measurement and the rest signal for the offset-locking. The cut-off frequency of the LPF between Mixer 2 and the two feedback PIDs is set to 270 kHz which determines the bandwidth of the offset-locking loop. The offset-locking beating method is a variant of the delayed self-heterodyne scheme for measuring the laser linewidth [21]. The FWHM linewidth of the beating signal reflects residual high-frequency fluctuations of the individual laser beyond the bandwidth of the offset-locking loop [18]. In our case the linewidth broadening due to frequency modulation is small compared to the initial

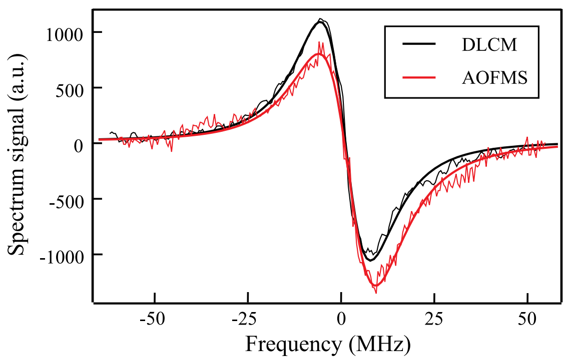

Fig. 2. DLCM and AOFMS spectra. Thin black (red) curves, measured spectrum of DLCM (AOFMS). Thick black (red) lines, fitting results with the fixed $\beta = 8$, $\omega_m = 100$ kHz, and $\phi = 0.91\pi$.

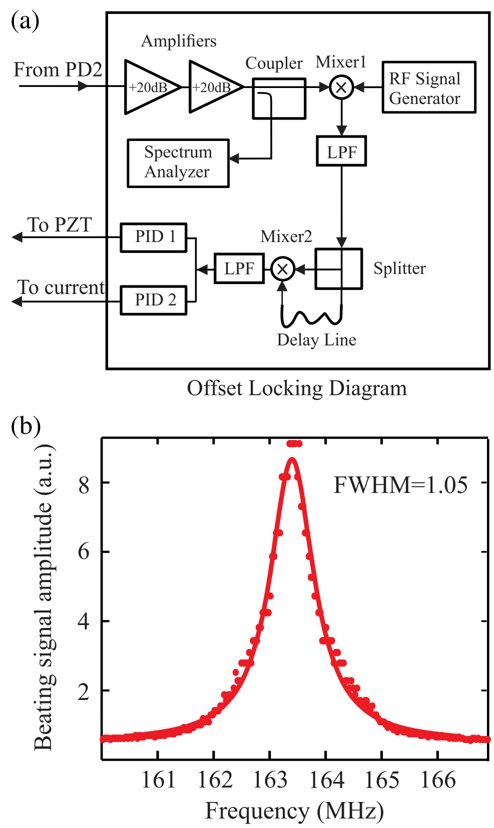

Fig. 3. Offset locking setup and the power spectrum of the beating signal; (a) offset-locking scheme; (b) typical power spectrum of the beating signal with the fitted FWHM is 1.05 MHz, showing the individual laser linewidth 525 kHz. Beating signal is taken by a GW Instek GSP-730 spectrum analyzer with 300 kHz resolution bandwidth and averaged over 200 sweeps of 500 ms each.

laser linewidth; the beating signal can be well-described by a Lorentzian profile as shown in Fig. 3. When the profile is Lorentzian, the laser FWHM linewidth is then given by the half of the beating FWHM linewidth [22].

C. Optimization of DLCM

When the modulation index decreases, the strength of the higher-orders' sideband decreases, resulting in a fast decay of the amplitude of the spectrum. The dependence of the amplitude of the DLCM spectrum on the modulation frequency ω_m is simulated and measured as shown in Fig. 4 by fixing $\Delta\omega$ at 1 MHz.

The simulation predicts a cut-off frequency of the amplitude at around 3.0 MHz, while our measurement shows that the decay appears at 500 kHz. The difference between the simulation and the measurement arises from the fact that the theoretical model does not include gas dynamics of atomic vapor [7,9,17]. Our experiment is implemented with 340°C lithium vapor, and the most probable speed of lithium atoms is about 1300 m/s. The gas dynamic effect significantly changes the atom–light interaction region when the beam waists of the pump and probe beams are small. With our beam diameter of 1.6 mm, based on a heuristic argument that the cut-off frequency is determined by the timescale where excited atoms escape the optical field of the pumped beam, the cut-off frequency will approximately at 800 kHz [9]. This estimation qualitatively explains the observed fast decay in our experiments. To search the optimal modulation index, we limit the modulation frequency lower than the decay threshold of 250 kHz.

We choose the modulation frequency $\omega_m = 100$ kHz to study the dependence of laser linewidth on the modulation index as shown in Fig. 5(a). For this small modulation frequency compared to the laser linewidth, we find that all the beating signal can be well-fitted by the Lorentzian profile when the modulation index β is less than 6. The laser FWHM linewidth shows a minimum value of 525 kHz at $\beta = 2$. In principle, the laser linewidth should decreases monotonically with the decrease of the modulation index β for a fixed modulation frequency. However, when β decreases, the amplitude of the DLCM spectrum also decreases. For $\beta = 2$, we measured the peak–peak amplitude of the spectrum decreases to 575 (a.u. in DigitLock) corresponding to the 10.9 MHz absorption linewidth. To stabilize the laser down to 500 kHz, the residue error

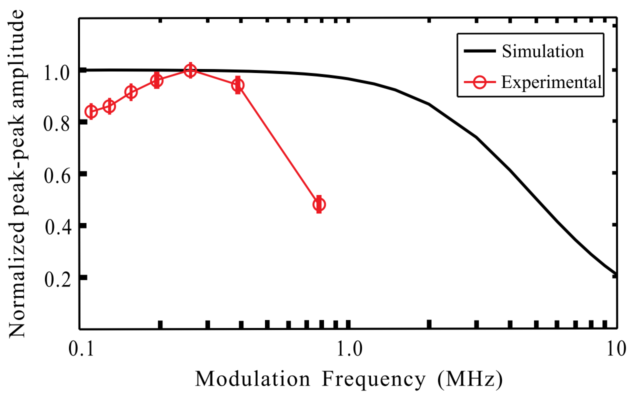

Fig. 4. Dependence of the amplitude of the DLCM signal on the modulation frequency with $\Delta\omega = 1$ MHz.

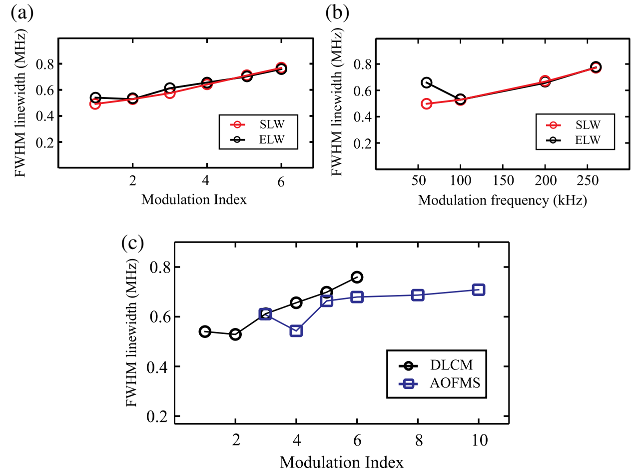

Fig. 5. Laser FWHM linewidth in terms of different modulation parameters; (a) dependence of the linewidth on the modulation index β for $\omega_m = 100$ kHz; (b) dependence of the linewidth on the modulation frequency ω_m for $\beta = 2$; (c) linewidth comparison between DLCM and AOFMS for $\omega_m = 100$ kHz. Black (red) open circles, experimental (simulated) linewidth for DLCM, where the simulation is calculated by the standard frequency modulated linewidth. Blue square, measured linewidth for AOFMS. Curves, simple joint lines.

signal is around 26 (a.u.), which approaches to the system noise limit of 12 (a.u., root-mean square value) in the DLCM spectrum. This analysis explains our observation that the further decreasing of β below 2 will increase the laser linewidth.

The modulation index $\beta = 2$ is then used to search the optimal value of the modulation frequency below the 250 kHz region. The dependence of the FWHM linewidth on the modulation frequency shows a minimum value at 100 kHz in Fig. 5(b). When the modulation frequency is below 100 kHz, the increase of the laser linewidth is induced by the decreased bandwidth of the servo loop.

We also compared the locking performance between the DLCM and the AOFMS as shown in Fig. 5(c). While the laser linewidth by the AOFMS locking almost has no dependence on the modulation index, it is limited the SNR of the spectrum as discussed in Section 4, Subsection A. The minimized laser linewidth is around 550 kHz, which shows that the DLCM method is comparable with the AOFMS one.

D. Long-Term Stability

In order to measure the frequency stability of DLCM in the long-term, we record the error signal before and after switching on the servo loop as shown in Fig. 6. The fluctuation of the laser frequency relative to the $2\,^2S_{1/2}, F = 3/2$ to $2\,^2P_{3/2}$ transition of ^{6}Li is estimated to be ± 10 MHz in the free-run stage. With the servo loop on, the RMS fluctuation linewidth is reduced to 0.5 MHz over more than 20 min. It demonstrates that the laser frequency noise is suppressed significantly in the long-term by the DLCM locking.

5. SUMMARY

A convenient and cost-efficient method is presented to stabilize the frequency of a tunable diode laser using DLCM-based

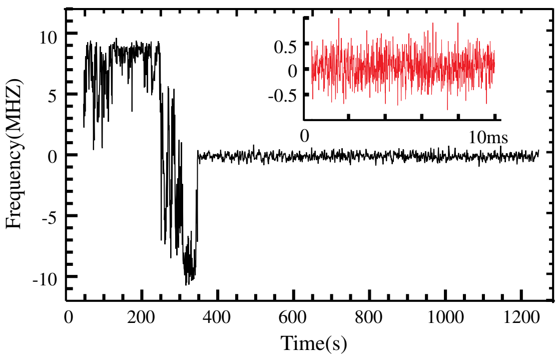

Fig. 6. Error signal of locking over the long-term. Inset, error signal in the short timescale after locking.

modulation transfer spectroscopy of an atomic vapor cell. The modulation transfer spectrum is simulated in detail by a theoretical model, and the high SNR of the spectrum is obtained by optimizing the modulation amplitude and frequency. By frequency-beating the stabilized laser and the offset-locking laser, we confirm that the laser linewidth can be reduced down to 500 kHz. This work realizes a digital current modulation scheme to stabilize the frequency of a tunable diode laser in sub-MHz regime without requiring additional optical modulators and can be easily adopted by many atomic physics and spectroscopy experiments.

8 Indiana University (RSFG2014); National Basic Research Program of China (2013CB922403); Purdue University (PRF2014).

Le Luo is a member of the Indiana University Center for Spacetime Symmetries (IUCSS). Le Luo thanks the support from Indiana University RSFG and Purdue University PRF. Tianshu Lai thanks the support from the National Basic Research Program of China (2013CB922403).

REFERENCES

1. L. Ricci, M. Weidemüller, T. Esslinger, A. Hemmerich, C. Zimmermann, V. Vuletic, W. König, and T. W. Hänsch, “A compact grating-stabilized diode-laser system for atomic physics,” Opt. Commun. **117**, 541–549 (1995).
2. C. E. Wieman and L. Hollberg, “Using diode lasers for atomic physics,” Rev. Sci. Instrum. **62**, 1–20 (1991).
3. M. S. Taubman and J. L. Hall, “Cancellation of laser dither modulation from optical frequency standards,” Opt. Lett. **25**, 311–313 (2000).
4. G. C. Bjorklund, “Frequency-modulation spectroscopy: a new method for measuring weak absorptions and dispersions,” Opt. Lett. **5**, 15–17 (1980).
5. G. C. Bjorklund, M. D. Levenson, W. Lenth, and C. Ortiz, “Frequency modulation (FM) spectroscopy,” Appl. Phys. B **32**, 145–152 (1983).
6. J. L. Hall, “Optical heterodyne saturation spectroscopy,” Appl. Phys. Lett. **39**, 680–682 (1981).
7. C. Bordé, J. Hall, C. Kunasz, and D. Hummer, “Saturated absorption line shape: Calculation of the transit-time broadening by a perturbation approach,” Phys. Rev. A **14**, 236–263 (1976).
8. J. F. Eble and F. Schmidt-Kaler, “Optimization of frequency modulation transfer spectroscopy on the calcium 4^1S_0 to 4^1P_1 transition,” Appl. Phys. B **88**, 563–568 (2007).
9. V. Negnevitsky and L. D. Turner, “Wideband laser locking to an atomic reference with modulation transfer spectroscopy,” Opt. Express **21**, 3103–3113 (2013).
10. Z. Zhang, X. Wang, and Q. Lin, “A novel way for wavelength locking with acousto-optic frequency modulation,” Opt. Express **17**, 10372–10377 (2009).
11. J. E. Debs, N. P. Robins, A. Lance, M. B. Kruger, and J. D. Close, “Piezo-locking a diode laser with saturated absorption spectroscopy,” Appl. Opt. **47**, 5163–5166 (2008).
12. S. Olmschenk, K. Younge, D. Moehring, D. Matsukevich, P. Maunz, and C. Monroe, “Manipulation and detection of a trapped Yb^+ hyperfine qubit,” Phys. Rev. A **76**, 052314–052323 (2007).
13. J. J. Snyder, R. K. Raj, D. Bloch, and M. Ducloy, “High-sensitivity nonlinear spectroscopy using a frequency-offset pump,” Opt. Lett. **5**, 163–165 (1980).
14. G. Camy, C. J. Bordé, and M. Ducloy, “Heterodyne saturation spectroscopy through frequency modulation of the saturating beam,” Opt. Commun. **41**, 325–330 (1982).
15. C. E. Shannon, “Communication in the presence of noise,” Proc. IRE **37**, 10–21 (1949).
16. E. Jaatinen, “Theoretical determination of maximum signal levels obtainable with modulation transfer spectroscopy,” Opt. Commun. **120**, 91–97 (1995).
17. T. M. Stace and A. N. Luiten, “Theory of spectroscopy in an optically pumped effusive vapor,” Phys. Rev. A **81**, 033848 (2010).
18. U. Schünemann, H. Engler, R. Grimm, M. Weidemüller, and M. Zielonkowski, “Simple scheme for tunable frequency offset locking of two lasers,” Rev. Sci. Instrum. **70**, 242–243 (1999).
19. L. D. Turner, K. P. Weber, C. J. Hawthorn, and R. E. Scholten, “Frequency noise characterisation of narrow linewidth diode lasers,” Opt. Commun. **201**, 391–397 (2002).
20. E. Bava, G. Galzerano, and C. Svelto, “Frequency-noise sensitivity and amplitude-noise immunity of discriminators based on fringe-side Fabry-Pérot cavities,” IEEE Trans. Ferroelect. Freq. Control **49**, 1150–1159 (2002).
21. N. Zhang, W. Rao, Z. Meng, P. Xu, Z. Hu, and C. Cao, “Linewidth study of the frequency-modulated laser based on the delayed self-heterodyne scheme,” Opt. Laser Technol. **45**, 267–271 (2013).
22. T. Okoshi, K. Kikuchi, and A. Nakayama, “Novel method for high resolution measurement of laser output spectrum,” Electron. Lett. **16**, 630–631 (1980).

Queries

1. AU: Edits to title OK (as per OSA style)?
2. AU: Are the author names correct as they are written?
3. AU: Only one author can be identified specifically as Corresponding author. Please confirm that the author e-mail information is correct as displayed.
4. AU: The Refs. [19, 20] is not cited in the article and also references are not cited in sequential order. Kindly provide the reference in sequential order.
5. AU: Does the acronym "AOM," mentioned in the sentence, "It usually stabilizes the laser linewidth…," refer to "acousto-optic modulation"?
6. AU: Please define all of the undefined terms in Eq. (1). Please also specify which, if any, of the terms are constant values (i.e., not variables).
7. AU: Please define the term "Re," mentioned in Eq. (2). Also, is this term a variable, or is it a constant value?
8. The funding information for this article has been generated using the information you provided to OSA at the time of article submission. Please check it carefully. If any information needs to be corrected or added, please provide the full name of the
356 funding organization/institution as provided in the FundRef Registry (http://www.crossref.org/fundref/fundref_registry.html).

Supplementary Material

This article has the following supplementary material items associated with it.